Anal. Chem. **2009,** *81,* 7988–8000

Fluorescent Thermometers for Dual-Emission-Wavelength Measurements: Molecular Engineering and Application to Thermal Imaging in a Microsystem

T. Barilero,[†] T. Le Saux,*[,†] C. Gosse,*[,‡] and L. Jullien*[,†]

Ecole Normale Supérieure, Département de Chimie, UMR CNRS-ENS-UPMC Paris 6 8640 Pasteur, 24, Rue Lhomond, 75005 Paris, France, and Laboratoire de Photonique et de Nanostructures, LPN-CNRS, Route de Nozay, 91460 Marcoussis, France

To facilitate thermal imaging, particularly in microdevices, one has to favor molecular thermometers in which the response is independent of the probe concentration and of the observation setup imperfections. Hence, this paper introduces two temperature fluorescent probes for ratiometric dual-emission-wavelength measurements in aqueous solutions. They are based on a nonathermal chemical reaction, either a conformational transition or a protonation, that induces a modification of their emission spectra as the temperature changes. Relying on both a straightforward theoretical analysis and thorough photophysical, thermodynamic, and kinetic investigations, we demonstrate how the flexible design of these two thermometers can be optimized to face applications with various requirements in terms of operating temperature and wavelength ranges as well as temporal resolution. For instance, the present molecules, which can be used between 5 and 35 °C, provide a relative sensitivity up to $\sim 9 \times 10^{-2}$ K^{-1} and milli- to microsecond response times. Finally, we utilize a two-color molecular beacon, a probe belonging to the first series of thermometers, to image temperature profiles in a microfluidic cell heated by a resistive strip. The ratiometric analysis of the fluorescence emission at two different wavelengths is performed on a widely available dual-view microscope, illustrating both the simplicity and reliability of the thermal mapping protocol.

Thermal issues have played an important role in the development and acceptation of microlaboratories. For instance, miniaturization of PCR vessels has enabled higher cycling speeds thanks to faster heating and cooling rates.[1,2] Independently, it has been shown that planar electrophoresis devices allowed for improved heat dissipation, thus limiting the detrimental outcomes of Joule effect on separation quality.[3,4] The ability to measure temperature in microfluidic devices was part of this success and will definitely stay a key technology. Indeed, steady-state thermal gradients and temporal temperature variations are involved in an increasing number of on-chip applications: control and measurement of enzymatic activity,[5−7] investigation of the thermodynamics[8,9] and of the kinetics[10,11] characterizing molecular associations (e.g., hybridization between complementary DNA strands). Additionally, the generation of a well controlled and defined temperature field is also crucial for several recently developed separation techniques: isoelectric focusing in a thermally generated pH gradient,[12] temperature gradient focusing,[13] and temperature gradient gel electrophoresis.[14]

Thermometric techniques are traditionally divided into contact and noncontact ones.[15] In the microfluidics context, the first group mainly consists of electrical sensors such as resistive thermal detector or thermocouples.[7,16,17] While precise and rapid if miniaturized, these invasive probes require additional microfabrication steps and can only perform punctual temperature measurements. In contrast, noncontact techniques usually yield a broad field view of the thermal exchanges occurring in a chip. They can be based on various physical effects. For example, IR thermography infers temperature from the device external surface

* To whom correspondence should be addressed. E-mail: Thomas.Lesaux@ens.fr (T.L.S.); Ludovic.Jullien@ens.fr (L.J.); charlie.gosse@lpn.cnrs.fr (C.G.).
[†] Ecole Normale Supérieure, Département de Chimie, UMR CNRS-ENS-UPMC Paris 6 8640.
[‡] Laboratoire de Photonique et de Nanostructures, LPN-CNRS.

(1) de Mello, A. J. *Lab Chip* **2001**, *1*, 24N–29N.
(2) The references selected for this introduction mainly focus on microfluidic device thermometry. Further readings would include reviews on either molecular thermometry[28−30] or on-chip thermal cycling technologies.[16]
(3) Manz, A.; Eijkel, J. C. T. *Pure Appl. Chem.* **2001**, *73*, 1555–1561.
(4) Petersen, N. J.; Nikolajsen, R. P. H.; Mogensen, K. B.; Kutter, J. P. *Electrophoresis* **2004**, *25*, 253–269.
(5) Tanaka, Y.; Slyadnev, M. N.; Hibara, A.; Tokeshi, M.; Kitamori, T. *J. Chromatogr., A* **2000**, *894*, 45–51.
(6) Mao, H.; Yang, T.; Cremer, P. S. *J. Am. Chem. Soc.* **2002**, *124*, 4432–4435.
(7) Arata, H. F.; Rondelez, Y.; Noji, H.; Fujita, H. *Anal. Chem.* **2005**, *77*, 4810–4814.
(8) Mao, H.; Holden, M. A.; You, M.; Cremer, P. S. *Anal. Chem.* **2002**, *74*, 5071–5075.
(9) Baaske, P.; Duhr, S.; Braun, D. *Appl. Phys. Lett.* **2007**, *91*, 133901.
(10) Braun, D.; Libchaber, A. *Appl. Phys. Lett.* **2003**, *83*, 5554–5556.
(11) Dodge, A.; Turcatti, G.; Lawrence, I.; de Rooij, N. F.; Verpoorte, E. *Anal. Chem.* **2004**, *76*, 1778–1787.
(12) Huang, T.; Pawliszyn, J. *Electrophoresis* **2002**, *23*, 3504–3510.
(13) Ross, D.; Locascio, L. E. *Anal. Chem.* **2002**, *74*, 2556–2564.
(14) Buch, J. S.; Kimball, C.; Rosenberger, F.; Highsmith, W. E., Jr.; DeVoe, D. L.; Lee, C. S. *Anal. Chem.* **2004**, *76*, 874–881.
(15) Childs, P. R. N.; Greenwood, J. R.; Long, C. A. *Rev. Sci. Instrum.* **2000**, *71*, 2959–2978.
(16) Zhang, C.; Xu, J.; Ma, W.; Zheng, W. *Biotechnol. Adv.* **2006**, *24*, 243–284.
(17) Gillot, F.; Morin, F. O.; Arata, H. F.; Guéguan, R.; Tanaka, H.; Fujita, H. *Lab Chip* **2007**, *7*, 1600–1602.

10.1021/ac901027f CCC: $40.75
Published on Web 08/27/2009

emissivity.[18,19] On the other hand, some methods make use of changes in the solvent structure. More precisely, as water heats up, Raman[20] and NMR[21] spectroscopies measure the dissociation of intermolecular hydrogen bonds whereas interferometric setups[22,23] detect the refractive index drop originating from dilation. However, none of these techniques offer a good enough spatial resolution to appropriately map fine fluidic structures. Thus, semi-invasive methods appear as a good compromise between contact and noncontact measurements: a molecular probe is introduced in the device and its response to temperature variations is monitored by optical microscopy, typically in the visible part of the spectra. For instance, heating modifies the hue of the cholesteric liquid crystals[24,25] and the birefringency of the nematic ones.[17,26] Although useful during prototyping, these materials are of limited interest for real time and in situ measurements because they are not soluble, especially in water. From the latter point of view, other probes such as thermochromic[27] and fluorescent molecules[28−30] provide valuable alternatives. They can be used down to micromolar concentrations and some of them are biocompatible,[31−33] a necessary property for applications in life sciences.

In their principle, most fluorescent thermometers (e.g., organic dyes such as rhodamine B,[33−38] inorganic complexes of ruthenium[39,40] or europium)[32,41] exploit the drop of their emission quantum yield with increasing temperature, a consequence of the thermal activation of a nonradiative deexcitation pathway.[29,30] In an imaging context, the spatial pattern of fluorescence intensity is then indicative of the temperature field in the solution containing the probe. However, precise temperature retrieval is here hampered by the additional dependence of the fluorescence signal on the thermometer concentration. Indeed, this parameter can be difficult to control because phenomena such as photobleaching, adsorption on the channel walls,[38] thermophoresis,[42,43] and/or thermally driven focusing[12,13] may deplete certain regions while enriching others. Two strategies are currently developed to overcome the latter limitation. The first one consists in relying on the emission lifetime[31,44−47] which depends on temperature but not on the probe concentration. In the second and instrumentally less demanding approach, the ratio between the temperature dependent emission at two different wavelengths enables to correct for spatial inhomogeneities due to uneven fluorescent thermometer distribution and/or experimental setup limitations (nonuniform excitation and/or light collection).[48]

Various experimental realizations have already been reported in ratiometric thermometry. Among them, dyes exhibiting delayed fluorescence,[49] thermographic phosphors,[50] excimers,[28,51,52] and band-dyes[53] are based on excited states engineering. Yet ground states engineering could also be explored because of its greater simplicity. In the present report, we adopt the latter strategy with the aim to design and to employ unimolecular fluorescent temperature probes for dual-emission-wavelength measurements in aqueous solutions. Our thermometers are molecules involved in a nonathermal chemical reaction and which exchanging states display different emission features. We first introduce the theoretical background necessary to establish a few simple rules yielding to optimized probes. Then, we present two versatile chemical platforms which can be implemented to easily build thermometers. More precisely, as in some previously published papers, we focused on either nucleic acids folding[11,54,55] or on protonation[10,34,42,43,47,56] to obtain the desired temperature driven alteration of the fluorescence emission. However, we are here able to perform ratiometric temperature measurements as we work with either a two-color molecular beacon[57−59] or with a fluorescent pH probe for dual-emission-wavelength measurements.[60,61] Finally,

(18) Roper, M. G.; Easley, C. J.; Legendre, L. A.; Humphrey, J. A. C.; Landers, J. P. *Anal. Chem.* **2007**, *79*, 1294–1300.
(19) Fudym, O.; Pradere, C.; Batsale, J.-C. *Chem. Eng. Sci.* **2007**, *62*, 4054–4064.
(20) Davis, K. L.; Liu, K.-L. K.; Lanan, M.; Morris, M. D. *Anal. Chem.* **1993**, *65*, 293–298.
(21) Lacey, M. E.; Webb, A. G.; Sweedler, J. V. *Anal. Chem.* **2000**, *72*, 4991–4998.
(22) Swinney, K.; Bornhop, D. J. *Electrophoresis* **2001**, *22*, 2032–2036.
(23) Easley, C. J.; Legendre, L. A.; Roper, M. G.; Wavering, T. A.; Ferrance, J. P.; Landers, J. P. *Anal. Chem.* **2005**, *77*, 1038–1045.
(24) Chaudhari, A. M.; Woudenberg, T. M.; Albin, M.; Goodson, K. E. *J. Microelectromech. Syst.* **1998**, *7*, 345–355.
(25) Iles, A.; Fortt, R.; de Mello, A. J. *Lab Chip* **2005**, *5*, 540–544.
(26) Aszódi, G.; Szabon, J.; Jánossy, I.; Székely, V. *Solid-State Electron.* **1981**, *24*, 1127–1133.
(27) Wätzig, H. *Chromatographia* **1992**, *33*, 445–448.
(28) Chandrasekharan, N.; Kelly, L. A. In *Reviews in Fluorescence*, Vol. 1; Geddes, C. D., Lakowicz, J. R., Eds.; Kluwer Academic/Plenum: New York, 2004; pp 21−40.
(29) Uchiyama, S.; Prasanna de Silva, A.; Iwai, K. *J. Chem. Educ.* **2006**, *83*, 720–727.
(30) Gosse, C.; Bergaud, C.; Löw, P. *Top. Appl. Phys.*, in press.
(31) Chapman, C. F.; Liu, Y.; Sonek, G. J.; Tromberg, B. J. *Photochem. Photobiol.* **1995**, *62*, 416–425.
(32) Zohar, O.; Ikeda, M.; Shinagawa, H.; Inoue, H.; Nakamura, H.; Elbaum, D.; Alkon, D. L.; Yoshioka, T. *Biophys. J.* **1998**, *74*, 82–89.
(33) Kato, H.; Nishizaka, T.; Iga, T.; Kinosita, K.; Ishiwata, S. *Proc. Natl. Acad. Sci. U.S.A.* **1999**, *96*, 9602–9606.
(34) Coppeta, J.; Rogers, C. *Exp. Fluids* **1998**, *25*, 1–15.
(35) Sakakibara, J.; Adrian, R. J. *Exp. Fluids* **1999**, *26*, 7–15.
(36) Ross, D.; Gaitan, M.; Locascio, L. E. *Anal. Chem.* **2001**, *73*, 4117–4123.
(37) Erickson, D.; Sinton, D.; Li, D. *Lab Chip* **2003**, *3*, 141–149.
(38) Samy, R.; Glawdel, T.; Ren, C. L. *Anal. Chem.* **2008**, *80*, 369–375.
(39) Sato, Y.; Irisawa, G.; Ishizuka, M.; Hishida, K.; Maeda, M. *Meas. Sci. Technol.* **2003**, *14*, 114–121.
(40) Filevich, O.; Etchenique, R. *Anal. Chem.* **2006**, *78*, 7499–7503.
(41) Kolodner, P.; Tyson, J. A. *Appl. Phys. Lett.* **1982**, *40*, 782–784.
(42) Braun, D.; Libchaber, A. *Phys. Rev. Lett.* **2002**, *89*, 188103.
(43) Duhr, S.; Arduini, S.; Braun, D. *Eur. Phys. J. E* **2004**, *15*, 277–286.
(44) Jeon, S.; Turner, J.; Granick, S. *J. Am. Chem. Soc.* **2003**, *125*, 9908–9909.
(45) Benninger, R. K. P.; Koç, Y.; Hofmann, O.; Requejo-Isidro, J.; Neil, M. A. A.; French, P. M. W.; de Mello, A. J. *Anal. Chem.* **2006**, *78*, 2272–2278.
(46) Hu, H.; Koochesfahani, M.; Lum, C. *Exp. Fluids* **2006**, *40*, 753–763.
(47) Wong, F. H. C.; Banks, D. S.; Abu-Arish, A.; Fradin, C. *J. Am. Chem. Soc.* **2007**, *129*, 10302–10303.
(48) An implementation of this technique with two fluorophores has also been reported. A first molecule which fluorescence emission varies with the temperature is used as a thermometer whereas a second one which fluorescence emission does not vary with the temperature is used as an internal reference.[13,34,35] Nevertheless, it should be noted that differences of the physicochemical features of the two dyes may here generate errors in data interpretation (for instance, a difference of the respective Soret coefficients, in the presence of temperature gradients, or of the nonspecific adsorption on system walls).
(49) Fister, J. C., III; Rank, D.; Harris, J. M. *Anal. Chem.* **1995**, *67*, 4269–4275.
(50) Wade, S. A.; Collins, S. F.; Baxter, G. W. *J. Appl. Phys.* **2003**, *94*, 4743–4756.
(51) Lou, J.; Finegan, T. M.; Mohsen, P.; Hatton, T. A.; Laibinis, P. E. *Rev. Anal. Chem.* **1999**, *18*, 235–284.
(52) Sun, K.; Yamaguchi, A.; Ishida, Y.; Matsuo, S.; Misawa, H. *Sens. Actuators, B* **2002**, *84*, 283–289.
(53) Schrum, K. F.; Williams, A. M.; Haerther, S. A.; Ben-Amotz, D. *Anal. Chem.* **1994**, *66*, 2788–2790.
(54) Tashiro, R.; Sugiyama, H. *Angew. Chem., Int. Ed.* **2003**, *42*, 6018–6020.
(55) Nellåker, C.; Wållgren, U.; Karlsson, H. *Clin. Chem.* **2007**, *53*, 98–103.
(56) Straub, A. E.; Seitz, W. R. *Anal. Chem.* **1993**, *65*, 1491–1492.
(57) Zhang, P.; Beck, T.; Tan, W. *Angew. Chem., Int. Ed.* **2001**, *40*, 402–405.

we make use of the DNA-based thermometer to map temperature profiles in a microdevice heated by a resistive strip, finding results in close agreement with the ones obtained by finite elements model (FEM) simulations. Noticeably, this last experiment is performed on a simple dual-view epifluorescence microscope,[62] showing that our strategy for thermal mapping provides a cheap but reliable alternative to more sophisticated approaches.[44,45,47]

THEORY

In its principle, the present approach for noncontact thermal imaging uses the dependence on temperature of the signal emitted by a probe which is submitted to a nonathermal chemical reaction. As soon as the optical features of the thermometer exchanging states are different, it is possible to retrieve temperature from the overall collected signal. This section aims at evaluating for the probe both thermodynamic and photophysical requirements to perform measurements with the best sensitivity.

We consider here the reaction between the two different states of the molecular thermometer:

$$A_1 \rightleftarrows A_2 \tag{1}$$

Such a process may explicitly refer to a unimolecular exchange (as in the MB case where A_1 is the closed configuration of a molecular beacon and A_2 its open configuration; vide infra) or, alternatively, it may model a bimolecular reaction involving reactants in excess (as in the PH case where the acidic form of the probe, A_1, reacts with the basic form of the buffer, B_2, to yield the basic form of the probe, A_2, and the acidic form of the buffer, B_1; vide infra).

Looking for an optical signal which linearly varies with each species concentration, we choose fluorescence emission as an example relevant for the following. Then, we introduce $I_{\mathrm{tot}}^{\lambda_{\mathrm{exc}},\lambda_{\mathrm{em}}}$, the total light intensity collected by the observation setup. Assuming that A_1 and A_2 are the only fluorescent molecules in solution, the measured signal reduces to $I_{A_1}^{\lambda_{\mathrm{exc}},\lambda_{\mathrm{em}}} + I_{A_2}^{\lambda_{\mathrm{exc}},\lambda_{\mathrm{em}}}$ and writes, at chemical equilibrium with regards to the reaction described by eq 1,

$$I_{\mathrm{tot}}^{\lambda_{\mathrm{exc}},\lambda_{\mathrm{em}}} = E^{\lambda_{\mathrm{exc}}} C^{\lambda_{\mathrm{em}}} \left(\frac{1}{1+K} Q_{A_1}^{\lambda_{\mathrm{exc}},\lambda_{\mathrm{em}}} + \frac{K}{1+K} Q_{A_2}^{\lambda_{\mathrm{exc}},\lambda_{\mathrm{em}}} \right) [A]_{\mathrm{tot}} \tag{2}$$

where $[A]_{\mathrm{tot}}$ is the total probe concentration, equal to $[A_1] + [A_2]$; $E^{\lambda_{\mathrm{exc}}}$ and $C^{\lambda_{\mathrm{em}}}$ are apparatus functions accounting for the illumination intensity and the photon collection efficiency, respectively; and the $Q_{A_i}^{\lambda_{\mathrm{exc}},\lambda_{\mathrm{em}}}$ are the brightnesses associated with the A_i emission at wavelength λ_{em} upon excitation at wavelength λ_{exc} (see Supporting Information). Finally, K is interpreted either as a true thermodynamic constant when considering a unimolecular exchange or as an apparent thermodynamic constant involving the concentrations of the reactants in excess when considering a bimolecular reaction.

A priori, the dependence of $I_{\mathrm{tot}}^{\lambda_{\mathrm{exc}},\lambda_{\mathrm{em}}}$ on the temperature T may originate from each of the terms contained in eq 2.[63] In fact, with appropriate molecular systems and in a relevant temperature range (vide infra and Supporting Information), the dominating contribution to the variation of $I_{\mathrm{tot}}^{\lambda_{\mathrm{exc}},\lambda_{\mathrm{em}}}$ with T results from K. Integration of the van't Hoff equation yields

$$K(T) = \exp\left[-\frac{\Delta_{\mathrm{r}}H}{R} \left(\frac{1}{T} - \frac{1}{T_{1/2}} \right) \right] \tag{3}$$

with R the perfect gas constant, $T_{1/2}$ the temperature at which $K = 1$, and $\Delta_{\mathrm{r}}H$ the enthalpy of the reaction in eq 1, assumed here to be nonvanishing and constant in the considered working range. For typical values of the latter parameter, K may vary by 10% per Kelvin (vide infra). In contrast, $E^{\lambda_{\mathrm{exc}}} \times C^{\lambda_{\mathrm{em}}}$ should be marginally affected by possible changes of refractive indices upon heating (vide infra). Similarly, $[A]_{\mathrm{tot}}$ only weakly decreases when the solvent dilates (for instance, it drops by ~0.02% in aqueous solutions when the temperature rises from 293 to 294 K).[64] Regarding the $Q_{A_i}^{\lambda_{\mathrm{exc}},\lambda_{\mathrm{em}}}$ terms, the quantum yield of fluorescence emission of the most current probes typically decreases at most by 1% per Kelvin,[65] yielding a smaller contribution to the temperature dependence than the one of K (vide infra). Eventually, in the MB case, minor conformational changes may also occur upon heating and therefore affect the fluorophore emission.[66−68] Nevertheless, this effect should be essentially eliminated by introducing a suitable linker between the reporting probe and the thermometer moiety.[67,68]

Ratiometric thermometry can be achieved when the optical properties of A_1 and A_2 are different. As underlined in the introduction, such protocols are advantageous as they make temperature extraction independent of the probe concentration, $[A]_{\mathrm{tot}}$, as well as on the knowledge of some of the optical transfer functions that characterize the observation setup. For instance, in standard spectrofluorimeters, where $C^{\lambda_{\mathrm{em}}}$ is corrected to not depend on λ_{em}, the ratio between the total intensities of fluorescence emission acquired at two different wavelengths, $I_{\mathrm{tot}}^{\lambda_{\mathrm{exc}},\lambda_1}/I_{\mathrm{tot}}^{\lambda_{\mathrm{exc}},\lambda_2}$, writes

$$\rho_{\lambda_{\mathrm{exc}}}^{\lambda_1/\lambda_2} = \frac{Q_{A_1}^{\lambda_{\mathrm{exc}},\lambda_1} + K Q_{A_2}^{\lambda_{\mathrm{exc}},\lambda_1}}{Q_{A_1}^{\lambda_{\mathrm{exc}},\lambda_2} + K Q_{A_2}^{\lambda_{\mathrm{exc}},\lambda_2}} \tag{4}$$

Remarkably, the present expression for $\rho_{\lambda_{\mathrm{exc}}}^{\lambda_1/\lambda_2}$ only relies on chemical and spectroscopic properties: K accounts for the first

(58) Marras, S. A. E.; Kramer, F. R.; Tyagi, S. *Nucleic Acids Res.* **2002**, *30*, e122.
(59) Ueberfeld, J.; Walt, D. R. *Anal. Chem.* **2004**, *76*, 947–952.
(60) Charier, S.; Ruel, O.; Baudin, J.-B.; Alcor, D.; Allemand, J.-F.; Meglio, A.; Jullien, L. *Angew. Chem., Int. Ed.* **2004**, *43*, 4785–4788.
(61) Charier, S.; Ruel, O.; Baudin, J.-B.; Alcor, D.; Allemand, J.-F.; Meglio, A.; Jullien, L.; Valeur, B. *Chem.—Eur. J.* **2006**, *12*, 1097–1113.
(62) Kinosita, K.; Itoh, H.; Ishiwata, S.; Hirano, K.; Nishizaka, T.; Hayakawa, T. *J. Cell Biol.* **1991**, *115*, 67–73.
(63) Otherwise specified by the use of the appropriate units, e.g., degrees Celsius, T always designates the absolute temperature.
(64) *CRC Handbook of Chemistry and Physics*, 82nd ed.; Lide, D. R., Ed.; CRC Press: Boca Raton, FL, 2001.
(65) Valeur, B. *Molecular Fluorescence Principles and Applications*; Wiley VCH: Weinheim, Germany, 2002.
(66) The conformation of single-stranded oligonucleotides is known to be affected by temperature. See for instance Cantor, C. R.; Schimmel, P. R. *Biophysical Chemistry, Part III. The Behavior of Biological Macromolecules*; Freeman: New York, 1980.
(67) Barsky, V.; Perov, A.; Tokalov, S.; Chudinov, A.; Kreindlin, E.; Sharonov, A.; Kotova, E.; Mirzabekov, A. *J. Biomol. Screen.* **2002**, *7*, 247–257.
(68) Liu, W.-T.; Wu, J.-H.; Li, E. S.-Y.; Selamat, E. S. *Appl. Environ. Microbiol.* **2005**, *71*, 6453–6457.

ones whereas the $Q_{A_i}^{\lambda_{exc},\lambda_{em}}$ brightnesses account for the second ones.

Retaining the K contribution as the sole source of temperature dependence in eq 4 (vide supra), $\rho_{\lambda_{exc}}^{\lambda_1/\lambda_2}$ sigmoidally varies with the temperature. For low enough K values where A_1 predominates, for instance at low enough temperature if the reaction in eq 1 is endothermal, one has $\rho_{\lambda_{exc},0}^{\lambda_1/\lambda_2} = Q_{A_1}^{\lambda_{exc},\lambda_1}/Q_{A_1}^{\lambda_{exc},\lambda_2}$. In contrast, $\rho_{\lambda_{exc},\infty}^{\lambda_1/\lambda_2} = Q_{A_2}^{\lambda_{exc},\lambda_1}/Q_{A_2}^{\lambda_{exc},\lambda_2}$ for large enough K values where A_2 is the major species, corresponding to a large enough temperature for an endothermal reaction. Noticeably, $\rho_{\lambda_{exc},0}^{\lambda_1/\lambda_2}$ and $\rho_{\lambda_{exc},\infty}^{\lambda_1/\lambda_2}$ depend on the shape of the fluorescence emission spectra of A_1 and A_2 but not on their absorption properties nor on their quantum yields of fluorescence emission. Furthermore, the variation of $\rho_{\lambda_{exc}}^{\lambda_1/\lambda_2}$ for a given temperature change is maximal at the inflection point. Looking for the value T_i where the second derivative of the emission intensities ratio cancels, one finds

$$T_i = \frac{\Delta_r H}{2R}\left(\frac{Q_{A_1}^{\lambda_{exc},\lambda_2} - K(T_i)Q_{A_2}^{\lambda_{exc},\lambda_2}}{Q_{A_1}^{\lambda_{exc},\lambda_2} - K(T_i)Q_{A_2}^{\lambda_{exc},\lambda_2}}\right) \quad (5)$$

with $K(T_i)$ defined according to eq 3. Temperature evaluation is here at the most precise, with an optimal sensitivity given by the slope of the $\rho_{\lambda_{exc}}^{\lambda_1/\lambda_2}(T)$ curve:

$$\left(\rho_{\lambda_{exc}}^{\lambda_1/\lambda_2}\right)'(T_i) = \frac{Q_{A_1}^{\lambda_{exc},\lambda_2}Q_{A_2}^{\lambda_{exc},\lambda_1} - Q_{A_1}^{\lambda_{exc},\lambda_1}Q_{A_2}^{\lambda_{exc},\lambda_2}}{(Q_{A_1}^{\lambda_{exc},\lambda_2} + K(T_i)Q_{A_2}^{\lambda_{exc},\lambda_2})^2}\frac{\Delta_r H}{RT_i^2}K(T_i) \quad (6)$$

In addition, the temperature is linearly related to $\rho_{\lambda_{exc}}^{\lambda_1/\lambda_2}$ around T_i (typically over ~10 °C; vide infra), which facilitates data analysis.

In the most general case, the expressions of T_i and $(\rho_{\lambda_{exc}}^{\lambda_1/\lambda_2})'(T_i)$ are not explicit. Consequently, a numerical or a graphical approach is required to optimize the $Q_{A_i}^{\lambda_{exc},\lambda_{em}}$, $\Delta_r H$, and $T_{1/2}$ parameters in order to design an efficient ratiometric thermometer at a chosen temperature T_i. Nevertheless, analytic expressions can be derived when the reaction in eq 1 generates a large enough thermal effect, which is highly desirable (vide infra). For $|2RT_i/\Delta_r H| \ll 1$, eq 5 yields

$$\frac{1}{T_i} = \frac{1}{T_{1/2}} - \frac{R}{\Delta_r H}\ln\left(\frac{Q_{A_1}^{\lambda_{exc},\lambda_2}}{Q_{A_2}^{\lambda_{exc},\lambda_2}}\right) \quad (7)$$

at the first order (see Supporting Information). Using eq 3, one then has

$$K(T_i) = \frac{Q_{A_1}^{\lambda_{exc},\lambda_2}}{Q_{A_2}^{\lambda_{exc},\lambda_2}} \quad (8)$$

from which eqs 4 and 6 can be transformed into eqs 9 and 10, respectively:

$$\rho_{\lambda_{exc}}^{\lambda_1/\lambda_2}(T_i) = \frac{1}{2}\left(\rho_{\lambda_{exc},\infty}^{\lambda_1/\lambda_2} + \rho_{\lambda_{exc},0}^{\lambda_1/\lambda_2}\right) \quad (9)$$

$$\left(\rho_{\lambda_{exc}}^{\lambda_1/\lambda_2}\right)'(T_i) = \left(\rho_{\lambda_{exc},\infty}^{\lambda_1/\lambda_2} - \rho_{\lambda_{exc},0}^{\lambda_1/\lambda_2}\right)\frac{\Delta_r H}{4RT_i^2} \quad (10)$$

Equation 10 provides simple guidelines to design efficient optical probes for ratiometric temperature measurements at T_i. Indeed, the highest sensitivity will be obtained if (i) one favors a reaction associated with a large enthalpy variation, (ii) one tunes the excitation and emission wavelengths such as $|(Q_{A_1}^{\lambda_{exc},\lambda_1}/Q_{A_1}^{\lambda_{exc},\lambda_2}) - (Q_{A_2}^{\lambda_{exc},\lambda_1}/Q_{A_2}^{\lambda_{exc},\lambda_2})|$ is maximized.

Equations 7−10 are noticeably analogous to the ones associated with the temperature dependence of $I_{tot}^{\lambda_{exc},\lambda_{em}}$ (see Supporting Information). Indeed, at the same order in the $|2RT_i/\Delta_r H| \ll 1$ regime, one finds $1/T_i = 1/T_{1/2}$, $K(T_i) = 1$,

$$I_{tot}^{\lambda_{exc},\lambda_{em}}(T_i) = \frac{1}{2}(I_{tot,\infty}^{\lambda_{exc},\lambda_{em}} + I_{tot,0}^{\lambda_{exc},\lambda_{em}}) \quad (11)$$

and

$$(I_{tot}^{\lambda_{exc},\lambda_{em}})'(T_i) = (I_{tot,\infty}^{\lambda_{exc},\lambda_{em}} - I_{tot,0}^{\lambda_{exc},\lambda_{em}})\frac{\Delta_r H}{4RT_i^2} \quad (12)$$

The similarity between the two sets of expressions underlines that a same origin, the occurrence of the eq 1 reaction, generates the temperature dependent behavior of both observables, $I_{tot}^{\lambda_{exc},\lambda_{em}}$ and $\rho_{\lambda_{exc}}^{\lambda_1/\lambda_2}$. In particular, for sensitive measurements the targeted operating range has to be centered on $T_{1/2}$, which is equal to T_i in one-color thermometry and close to it in two-color protocols where large $\Delta_r H$ values have been favored (see eq 7). However, the ratiometric approach is significantly more flexible. Indeed, eq 7 shows that various T_i values can be generated around $T_{1/2}$ by tuning λ_2. For instance, two different inflection temperatures are obtained by permuting λ_1 and λ_2, i.e., respectively, measuring $\rho_{\lambda_{exc}}^{\lambda_1/\lambda_2}$ and $\rho_{\lambda_{exc}}^{\lambda_2/\lambda_1}$, whereas only one inflection point, at $T_{1/2}$, can be used while observing $I_{tot}^{\lambda_{exc},\lambda_{em}}$.

EXPERIMENTAL SECTION

Reagents and Solutions. The MB, MBD, MBA, OD, and OA oligonucleotides were synthesized, labeled, and HPLC-purified by IBA (Göttingen, Germany). With the use of a 5′−3′ orientation, as well as *fam* and *tr* to, respectively, designate the Fluorescein and the Texas-Red fluorophores, their sequences read MB = *fam*-T_7-**GATAG**-T_{16}-**CTATC**-*tr*; MBD = *fam*-T_7-**GATAG**-T_{16}-**CTATC**; MBA = T_7-**GATAG**-T_{16}-**CTATC**-*tr*; OD = *fam*-T_7-GATAG-T_{21}; OA = T_{28}-CTATC-*tr*. The bases in bold are the ones involved in the stem formation. Additionally, the detailed structure of the linkers between the labels and the oligonucleotides backbone is provided in Scheme S-1 in the Supporting Information. PYMPON has been synthesized as already reported.[61] Poly(dimethylacrylamide) (PDMA) of average molecular weight 3 MDa was a kind gift of J. Weber (Institut Curie, Paris, France).

Solutions were prepared using water purified through a Direct-Q 5 (Millipore, Billerica, MA). The 0.1 M NaCl 10 mM Hepes buffer, pH 7.5 at 20 °C, was obtained by diluting stock solutions down to the following concentrations: NaCl 0.1 M, NaOH 5 mM, and Hepes 10 mM. To prevent probe adsorption onto surfaces, this solution was supplemented with 0.1% PDMA w/v when experiments were carried out in microdevices. The 5 mM

sodium monophthalate/sodium diphthalate buffer, pH 5.2 at 20 °C, was obtained by dissolving phthalic acid and sodium hydroxide in water at the following concentrations: phthalic acid 5 mM and NaOH 7.5 mM. The Britton-Robinson buffers were prepared according to Frugoni.[69]

UV−Visible Absorption and Steady-State Emission Spectroscopies. UV−vis absorption spectra were recorded on a Uvikon-940 spectrophotometer (Kontron, Zürich, Switzerland), and corrected fluorescence spectra were acquired on a LPS 220 spectrofluorometer (PTI, Monmouth Junction, NJ). The quartz cuvettes were, respectively, 1 cm × 1 cm and 2 mm × 1 cm. The holders were thermostatted using circulating baths (Polystat 34-R2, Fisher Bioblock Scientific, Illkirch, France), and the temperature was directly measured in the cuvettes using a type K thermocouple connected to a ST-610B digital pyrometer (Stafford Instruments, Stafford, U.K.). The temperatures T at which UV−vis absorption and emission spectra have been recorded in Figure 2 were the following: T = 21, 25, 29, 33, 38, 41, 44, 45, and 50 °C (Figure 2a); T = 7.3, 8.6, 10.0, 11.1, 12.5, 14.0, 15.7, 17.1, 18.4, 19.8, 21.2, 22.8, 24.3, 26.0, 27.5, 29.0, 30.5, 32.0, 33.5, and 36.5 °C (Figure 2b); T = 4.0, 6.0, 9.4, 12.3, 16.3, 20.4, 24.8, 29.4, 34.0, 38.0, 42.9, 46.9, 51.1, 55.3, 59.9, 64.3, 68.8, 73.3, 78.0, and 82.1 °C (Figure 2c); T = 3.4, 6.4, 9.8, 14.0, 17.3, 21.1, 24.8, 28.5, 32.4, 36.5, 40.4, 44.4, 48.1, 51.9, 55.3, 59.5, and 62.5 °C (Figure 2d).

Care was taken in order to always record spectra of reactive mixture at equilibrium. More precisely, we always used relative heating and cooling rates slower than the relaxation rate of the reaction in eq 1:[70] the temperature was varied at less than 10^{-2} °C/s whereas the relaxation rate had been independently evaluated at 5×10^4 s^{-1} for MB and 5×10^5 s^{-1} for PH (vide infra). Thus, for a given temperature, spectroscopic data obtained upon heating and upon cooling were identical (see Figure S-9 in the Supporting Information).

Device Microfabrication. An indium tin oxide (ITO) heater of length ℓ = 800 μm and width w = 20 μm was microfabricated onto a D263 glass wafer of thickness H = 470 μm (OPA Opticad, Mitry-Mory, France). As previously reported,[71] this is a four step process. First, an ITO layer of thickness $t \sim$ 400 nm and of resistivity ~ 7.5 Ω/□ was deposited onto the 470 μm thick, 2 in. diameter, glass substrate by cathodic sputtering (ACM, Villiers-S^t-Frédéric, France). Second, with the use of standard photolithography protocols, the heaters features were patterned in a 1.3 μm thick AZ 5214E layer (MicroChemicals, Ulm, Germany) as to define a mask for the subsequent etching of the ITO thin film. This operation was performed in an Ar^+ ion beam etching machine and followed by the resist mask removal in an acetone ultrasonic bath. Third, Au/Ge ohmic contacts were fabricated as to connect the microheaters to the macroscopic electrical circuit. A standard lift-off technology was used: features were defined in an AZ nLOF2070 layer (MicroChemicals) by optical lithography, metal films were next deposited by e-beam evaporation, and the resist was finally dissolved in acetone. A contact resistance between 10^{-5} and 5×10^{-5} Ω cm^2 could be obtained after annealing under reductive atmosphere (400 °C for 4 min). Fourth, the central part of the device, i.e., the one which will be in contact with the aqueous solution, was encapsulated in a 800 nm thick silica layer using plasma enhanced chemical vapor deposition. This last operation will prevent any electrokinetic phenomena and current leakage during heater operation.

Finally, the microsystem fabrication was completed by sandwiching two strips of parafilm (Pechiney Plastic Packaging, Chicago, IL) between the upper surface of the previously processed wafer and a ~140 μm thick D263 glass coverslip (Menzel-Gläser, Braunschweig, Germany). Watertight sealing was subsequently obtained by annealing on a hot plate (220 °C for 2 s). The resulting fluidic chamber was 4 mm large and 22 mm long, it had a height $\mathscr{H}$ = 130 μm (see Scheme S-3 in the Supporting Information).

Instrumentation and Video Microscopy. The device was mounted in series with a 47 Ω power resistor (RLP10 1%; Vishay-Sfernice, Selb, Germany) and connected to an AL991S stabilized power supply (ELC, Annecy, France). The voltage drop across the resistor, measured with a 5492 multimeter (B+K Precision, Yorba Linda, CA), could then be used to compute the constant current i flowing through the ITO strip.

The bottom glass surface of the microsystem was placed on a 0.8 mm thick copper slide in which a trench (2 mm large) had been dug for observation with the microscope. This holder was then mounted on an aluminum block thermostatted with a ±0.2 K precision by two thermoelectric Peltier devices (CP 1.0-63-05 L-RTV; Melcor, Trenton, NJ). The temperature was monitored using a TCS610 thermistor (Wavelength Electronics, Bozeman, MT) and the feedback loop was driven by a MPT10000 temperature controller (Wavelength Electronics) which received settings from the computer through a usb-1208FS I/O board (Measurement Computing, Norton, MA).

Two-color imaging was achieved at 24 Hz on a homemade dual-view microscope (see Scheme S-2 in the Supporting Information).[62] The light from the excitation source (a 100 W Xe lamp; LOT-Oriel, Palaiseau, France) was first reflected on a wide band hot mirror (FM01; Thorlabs, Newton, NJ) and passed through a filter for selective excitation of fluorescein (HQ 480/40; Chroma Technology, Rockingham, VT). Epifluorescence illumination was performed using a Q505 LP dichroic mirror (Chroma Technology) and a 10× objective (Fluar NA 0.5; Zeiss, Le Pecq, France). The collected light was then divided in two beams by a first 585DCXR dichroic mirror (Chroma Technology). The resulting channels, associated with both green and red colors, were subsequently individually filtered with the appropriate band-pass filters: either a HQ535/50 (Chroma Technology) or a D620/40 (Chroma Technology). Eventually, the final two-color image was assembled on a single CCD camera chip (Luca-R; Andor Technology, Belfast, Nothern Ireland) with the help of a second 585DCXR dichroic mirror. The field of view was ~0.5 mm for each channel, and images were recorded by averaging over 240 frames (corresponding to a 10 s integration time). Interfacing of the temperature controllers as well as video acquisition were performed using a homemade program written in C.

Three two-color images are necessary for thermal mapping. They were acquired and processed as follow. First, the setup was thermostatted at 293 K, the microchamber was filled with buffer,

(69) Frugoni, C. *Gazz. Chim. Ital.* **1957**, *87*, 403–407.
(70) Rougée, M.; Faucon, B.; Mergny, J.-L.; Barcelo, F.; Giovannangeli, C.; Garestier, T.; Hélène, C. *Biochemistry* **1992**, *31*, 9269–9278.
(71) Barilero, T.; Chapuis, P.-O.; Pujade, D.; Guilet, S.; Croquette, V.; Jullien, L.; Volz, S.; Gosse, C. *Transducers'07 & Eurosensors XXI, Digest of the Technical Papers* **2007**, U933–U934.

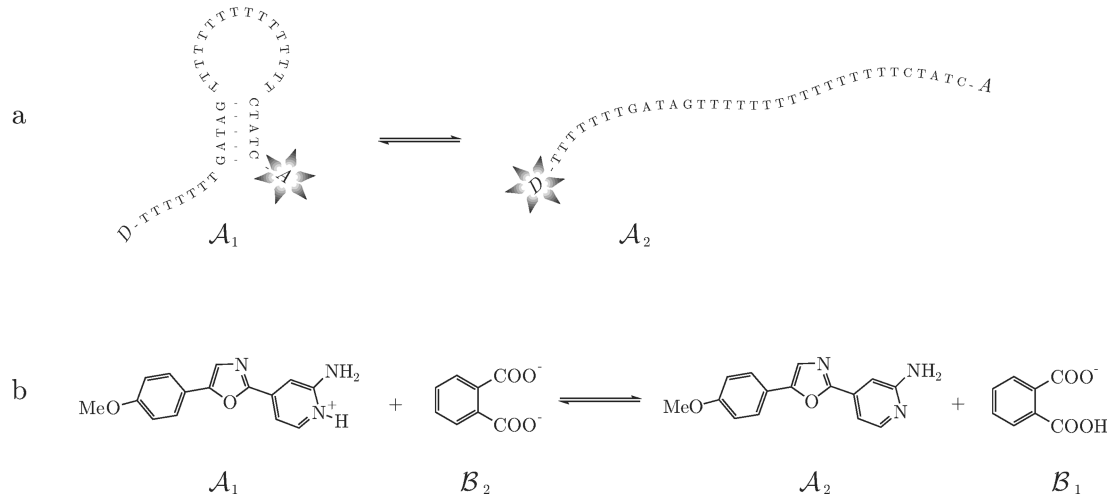

Figure 1. Two probes for ratiometric fluorescence emission measurement of the temperature. (a) The molecular beacon platform MB: In the A_1 closed state, which is stable at the lowest temperatures, the two fluorophores engaged in energy transfer (i.e., the Fluorescein *D* and Texas-Red *A*) are in close proximity. Hence, upon exciting the donor, one essentially collects fluorescence emission from the acceptor. In contrast, at the largest temperatures the A_2 open state is favored, the two fluorophores are distant, and the donor excitation essentially results in the donor emission. (b) The proton exchange platform PH: Upon deprotonation by the diphthalate basic form of the buffer $\mathcal{B}_2$, the A_1 acidic state of the fluorescent pH probe PYMPON provides the monophthalate ion $\mathcal{B}_1$ and the corresponding basic PYMPON state A_2, which emits fluorescence in a different wavelength range than A_1.

and a background image $\mathcal{B}^{\{\lambda_1,\lambda_2\}}_{\lambda_{exc},293K}(x,y)$ was recorded. Second, the solution was changed for buffer containing MB to yield a reference thermal image $\mathcal{T}^{\{\lambda_1,\lambda_2\}}_{\lambda_{exc},293K}(x,y)$. Eventually, the temperature field was modified, and the thermal image associated with the new experimental conditions, $\mathcal{T}^{\{\lambda_1/\lambda_2\}}_{\lambda_{exc}}(x,y)$, was acquired. The latter thermal perturbations were 2-fold in the present paper. On one hand, we changed the Peltier heat pumps settings by increments as to record the $\rho^{\lambda_1/\lambda_2}_{\lambda_{exc}}(T)$ calibration curve. On the other hand, an ITO strip was flowed with a current *i* as to map the temperature field around a micrometer-size heater. Subsequently, the background image $\mathcal{B}^{\{\lambda_1,\lambda_2\}}_{\lambda_{exc},293K}(x,y)$ was subtracted from both thermal images, $\mathcal{T}^{\{\lambda_1,\lambda_2\}}_{\lambda_{exc},293K}(x,y)$ and $\mathcal{T}^{\{\lambda_1,\lambda_2\}}_{\lambda_{exc}}(x,y)$, to correct them from the camera dark noise and parasite illumination. The resulting data were then divided by each other since in the present protocol the temperature map is determined with respect to a 293 K reference signal (see the Supporting Information). It thus yielded $[\mathcal{T}^{\{\lambda_1,\lambda_2\}}_{\lambda_{exc}}(x,y) - \mathcal{B}^{\{\lambda_1,\lambda_2\}}_{\lambda_{exc},293K}(x,y)]/[\mathcal{T}^{\{\lambda_1,\lambda_2\}}_{\lambda_{exc},293K}(x,y) - \mathcal{B}^{\{\lambda_1,\lambda_2\}}_{\lambda_{exc},293K}(x,y)]$ from which the fields of view associated with both red and green channels were cut out and the normalized ratiometric image, $\mathcal{R}^{\{\lambda_1,\lambda_2\}}_{\lambda_{exc}}(x,y)/\mathcal{R}^{\{\lambda_1,\lambda_2\}}_{\lambda_{exc},293K}(x,y)$, computed by division.

Data Processing. Otherwise specified, data have been processed and globally fitted with Igor Pro 6 (WaveMetrics, Lake Oswego, OR).

RESULTS AND DISCUSSION

MB and PH as Fluorescent Thermometers for Ratiometric Fluorescence Emission Measurements. In the present account, we introduce two different probes to measure temperature by using their ratio of fluorescence emission intensities at two different wavelengths. They have been conceived as to present an operating range laying around room temperature.

The first design, MB, relies on a DNA molecular beacon.[72] In reference to the reaction in eq 1, spontaneous exchange occurs between a closed state A_1, displaying a stem and a loop, and an open form A_2 (Figure 1a). As we will see, the molecular beacon platform is particularly favorable to implement the strategy exposed above. First, the structure opening is strongly endothermal. Then, several reliable programs are available to evaluate the thermodynamic features associated with stem pairing: various oligonucleotide sequences can be screened during the design step to get a probe exhibiting a desired $T_{1/2}$ value, typically ranging between a few to a few tens of degrees Celsius.[73,74] Eventually, labeling of the beacon extremities by a pair of fluorophores engaged in fluorescence resonant energy transfer (FRET) confers appropriate photophysical properties for a ratiometric analysis.[57−59] Indeed, the loop opening can cause the average distance between the donor *D* and the acceptor *A* to overcome the Förster radius (for which *D* excitation is equiprobably followed by *D* emission and by energy transfer to *A*).[65] MB, the molecular beacon retained in the present study, has been designed according to the previous rules to yield an optical thermometer working around room temperature (vide infra). Adopting the Fluorescein/Texas-Red *D*/*A* pair, we sought for a probe which, upon *D* excitation, should essentially emit *A* or *D* fluorescence according to the temperature, below or above $T_{1/2}$, respectively. More precisely, considering that the Förster distance is here equal to 5.6 nm (see the Supporting Information), we used the available programs[73] to engineer an oligonucleotide combining a large enough loop, in order to observe a significant change of the average interchromophore distance upon opening, and two complementary sequences yielding the formation of a stem that melts around 20−25 °C. It finally resulted in a 33 bp long single-strand DNA bearing the Fluorescein and Texas-Red fluorophores at its extremities and exhibiting a 5 bp-long stem at the lowest temperatures (see Figure 1a and Experimental Section).

(72) Tyagi, S.; Kramer, F. R. *Nat. Biotechnol.* **1996**, *14*, 303–308.

(73) Zuker, M. *Nucleic Acids Res.* **2003**, *31*, 3406–3415. http://mfold.bioinfo.rpi.edu/.

(74) SantaLucia, J., Jr.; Hicks, D. *Annu. Rev. Biophys. Biomol. Struct.* **2004**, *33*, 415–440.

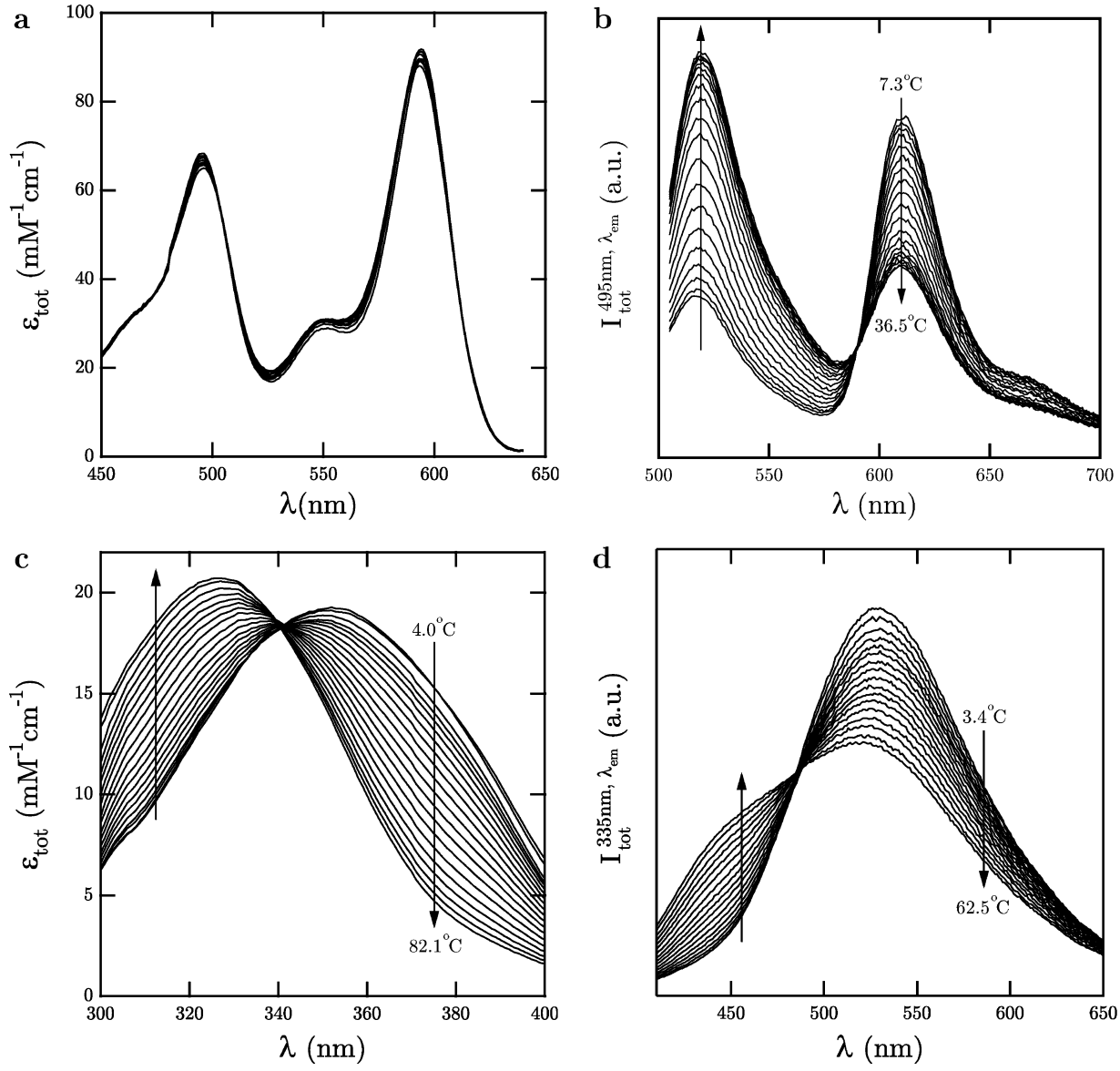

Figure 2. Temperature dependence of the absorption and emission spectra of MB and PH. (a) Evolution of the MB absorption spectrum in the 450−650 nm range. [MB] = 5 μM in 0.1 M NaCl 10 mM Hepes buffer, pH 7.5 at 20 °C. (b) Evolution of the MB emission spectrum upon excitation at λ_{exc} = 495 nm. [MB] = 50 nM in 0.1 M NaCl 10 mM Hepes buffer, pH 7.5 at 20 °C. (c) Evolution of the PH absorption spectrum in the 300−400 nm range. [PH] = 13 μM in 5 mM sodium monophthalate/sodium diphthalate buffer, pH 5.2 at 20 °C. (d) Evolution of the PH emission spectrum upon excitation at λ_{exc} = 335 nm. [PH] = 100 nM in 5 mM sodium monophthalate/sodium diphthalate buffer, pH 5.2 at 20 °C. See the Experimental Section for the temperatures at which spectra were collected.

The second design, PH, relies on a proton exchange reaction between an appropriate pair of reactants: the fluorescent pH probe PYMPON[60,61] and the monophthalate/diphthalate buffer (Figure 1b). The acidic state of PYMPON, A_1 in reference to the reaction in eq 1, and the monophthalate anion, B_1, exhibit similar protonation constants at 298 K: $pK_a(A_1) = 5.8 \pm 0.1$[60] and $pK_a(B_1) = 5.4$ (at zero ionic strength).[75] Thus, with a buffer containing identical concentrations of mono- and diphthalate, $T_{1/2}$ was anticipated to lie in the room temperature range. Indeed, the thermodynamic constant K here identifies to $(K_a(A_1) \times [B_2])/(K_a(B_1) \times [B_1])$, where $[B_1]$ and $[B_2]$ designate the concentrations in B_1 and B_2, assumed to be constant. In addition, the reaction enthalpies associated with the proton loss from the acidic states were chosen to exhibit opposite signs and thus maximize $\Delta_r H$: at 298 K the reported value for the pyridinium, which corresponds to the PYMPON headgroup, is 18.2 kJ mol^{-1} [76] whereas the one associated with the monophthalate anion is −2.2 kJ mol^{-1}.[75] Eventually, PYMPON exhibits a major shift in its fluorescence emission spectrum when protonated. This feature, which we already used to perform pH measurements by a ratiometric treatment of the fluorescence emission, here opens the road to thermometry using a similar approach.

Temperature Dependence of the MB Fluorescence Emission. Figure 2a displays the evolution of the MB absorption spectrum as a function of temperature in 0.1 M NaCl 10 mM

(75) Goldberg, R. N.; Kishore, N.; Lennen, R. M. *J. Phys. Chem. Ref. Data* **2002**, *31*, 231–370.

(76) Perrin, D. D. *Dissociation Constants of Organic Bases in Aqueous Solution: Supplement 1972*, Butterworths: London, 1972.

Hepes buffer, pH 7.5 at 20 °C. Between 450 and 650 nm, the absorption spectrum exhibits two bands, respectively, associated with Fluorescein ($\lambda_{absD}^{max} = 495$ nm) and Texas-Red ($\lambda_{absA}^{max} = 594$ nm); they are indeed close to the ones of the parent chromophores. Additionally, in the considered wavelength range the absorption spectrum is essentially independent of the temperature. In fact, the minor decrease of absorbance upon heating is in line with the positive thermal expansion coefficient of water:[64] the MB concentration decreases when the solvent dilates. Finally, the linkers prevent any considerable coupling between the terminal chromophores and the nucleic bases, making the absorption of the formers independent of any conformational change affecting the DNA backbone.[77]

Figure 2b displays the corresponding evolution of the MB steady-state fluorescence emission as a function of T upon exciting the Fluorescein chromophore ($\lambda_{exc} = 495$ nm). One observes the presence of two emission bands, respectively, associated with Fluorescein ($\lambda_{emD}^{max} = 518$ nm) and Texas-Red ($\lambda_{emA}^{max} = 610$ nm). In contrast to the behavior in absorption, the fluorescence emission spectrum of the molecular beacon strongly depends on temperature. When this latter parameter increases, the fluorescence emission from Fluorescein increases whereas the one from Texas-Red decreases. These observations are in line with the previously detailed expectations.

Design Rules and Optimization of Operating Conditions for MB. In relation to MB design, complementary experiments have been performed to further appreciate the preceding behavior in fluorescence emission. First, we concluded about the absence of any significant intrinsic dependence on temperature of the fluorescence emission from Fluorescein and Texas-Red by investigating the behavior of two MB analogues, OD and OA, which cannot form a stem and contain only one fluorophore, either Fluorescein or Texas-Red (Figure S-1 in the Supporting Information).

Then, we globally fitted the evolution in Figure 2b using eqs 2 and 3. We extracted $\Delta_r H = 169 \pm 2$ kJ mol^{-1} and $T_{1/2} = 290.3 \pm 0.1$ K (17.2 ± 0.1 °C) whereas, using M-Fold,[73] we anticipated $\Delta_r H = 173$ kJ mol^{-1} and $T_{1/2} = 307.1$ K (34.0 °C) in the presence of 0.1 M Na^+. The observed discrepancy for $T_{1/2}$ (a few percent range in Kelvin) probably originates from the presence of the terminal fluorophores which are not included in the predictions. Nevertheless, from the thermometer design point of view, such a variation is not a major drawback to make reliable measurements. Indeed λ_1 and λ_2 can be tuned to bring T_i in the desired temperature range (vide infra).

Additionally, the above fit of the Figure 2b data also provides the steady-state emission spectra of A_1 and A_2, the MB closed and open states which can, respectively, be observed at low and high temperature. They have been scrutinized for their consistency with the expected conformational changes. In particular, we evaluated the respective quantum yields of energy transfer from Fluorescein to Texas-Red in both states. We found $\phi_{A_1}^T \approx 80\%$ and $\phi_{A_2}^T \approx 30\%$ (see the Supporting Information). These values have then been converted into average distances between the Fluorescein and Texas-Red fluorophores, $\langle r_{A_i}^{DA} \rangle$, by assuming the energy transfer to be controlled by the Förster mechanism. It leads to $\langle r_{A_1}^{DA} \rangle = 4.4$ nm and $\langle r_{A_2}^{DA} \rangle = 6.4$ nm. Taking into account the length of the linkers between the fluorophores and the oligonucleotide backbone, such distances are in reasonable agreement with the expectations from MB pairing: in the closed A_1 state, both fluorophore cores are separated by 48 σ bonds plus 7 phosphorodiester bonds whereas this separation is increased by 26 phosphorodiester bonds in the open A_2 state (Figure 1a). Moreover, the Förster distance for the Fluorescein/Texas-Red couple, 5.6 nm, is located in the middle of the [$\langle r_{A_1}^{DA} \rangle$, $\langle r_{A_2}^{DA} \rangle$] range to get a major change of the emission spectrum upon rising temperature.

Altogether, the thermodynamic and photophysical information thus support the relevance of the present MB design to yield an optical thermometer based on ratiometric analysis of the fluorescence emission spectrum around room temperature. Moreover, the extracted thermodynamic parameters $\Delta_r H$ and $T_{1/2}$ satisfy $|2RT_i/\Delta_r H| \ll 1$. Thus, one can use the simplified eqs 7 and 10 to eventually identify the most appropriate excitation and emission wavelengths for measuring temperature with an optimal sensitivity. In the present situation, based on energy transfer, signal-to-noise ratio may govern the choice of the excitation wavelength. Consequently, we selected $\lambda_{exc} = 495$ nm to get a strong absorption of Fluorescein without any significant direct excitation of Texas-Red. Relying on eqs 7 and 10, we plotted on Figure S-3a,b in the Supporting Information the theoretical dependences of T_i and $(\rho_{\lambda_{exc}}^{\lambda_1/\lambda_2})'(T_i)$ on the wavelengths of fluorescence emission λ_1 and λ_2. Figure S-3a in the Supporting Information shows that an appropriate λ_2 value can always be found to perform thermometry around T_i between 12 and 20 °C. In addition, Figure S-3b in the Supporting Information evidences that the corresponding measurement is at the most sensitive when λ_1 is associated with the emission maxima of either Fluorescein if $T_i \gtrsim 16$ °C or Texas-Red if $T_i \lesssim 16$ °C. More specifically, a first optimum setting can be found at $T_i = 18.4$ °C where one has $(\rho_{\lambda_{exc}}^{\lambda_1/\lambda_2})'(T_i)/\rho_{\lambda_{exc}}^{\lambda_1/\lambda_2}(T_i) = 7.0 \times 10^{-2}$ K^{-1} using $\lambda_1 = 519$ nm and $\lambda_2 = 700$ nm. Alternatively, a second optimum can be found at $T_i = 12.8$ °C where one has $(\rho_{\lambda_{exc}}^{\lambda_1/\lambda_2})'(T_i)/\rho_{\lambda_{exc}}^{\lambda_1/\lambda_2}(T_i) = -8.8 \times 10^{-2}$ K^{-1} using $\lambda_1 = 611$ nm and $\lambda_2 = 573$ nm.

Being interested in thermometry over a wider operating range, we conversely computed $(\rho_{\lambda_{exc}}^{\lambda_1/\lambda_2})'(T)$ at any temperature between 4 and 36 °C to identify the λ_1 and λ_2 values yielding the best sensitivity. In fact, we found that the optimal wavelengths were identical to the ones required for working at T_i. Figure 3a eventually displays the corresponding dependence of the ratio of fluorescence emission, i.e., the $\rho_{495}^{519/700}(T)$ and $\rho_{495}^{611/573}(T)$ curves, around room temperature. Interestingly we noticed that in the $\{\lambda_1,\lambda_2\}$ couple resulting from the preceding optimization process, one of the wavelengths is always close to the maximum of emission of either Fluorescein or Texas-Red, whereas the other one is always located in a range where it generates low

(77) Noticeably, we did not notice any major alteration of the absorption spectrum between 250 and 300 nm, a wavelength range dominated by the contribution of the DNA bases. Beyond the coupling effects evoked above, this observation could contradict the 5 bp unpairing associated with stem melting (duplex dissociation results in hyperchromism, see Cantor and Schimmel[66]). However, one has to keep in mind that this alteration concerns only 10 bases whereas the molecular beacon is altogether 33 bp long.

(78) Although the PH relative sensitivity does not reach the peak value displayed by MB around its $T_{1/2}$, it is constant over a large temperature range. Therefore, the acid−base system enables thermometry nearly between 0 and 100 °C. In comparison, measurements with molecular beacons become poorly sensitive at temperatures departing by more than 20 °C from $T_{1/2}$.

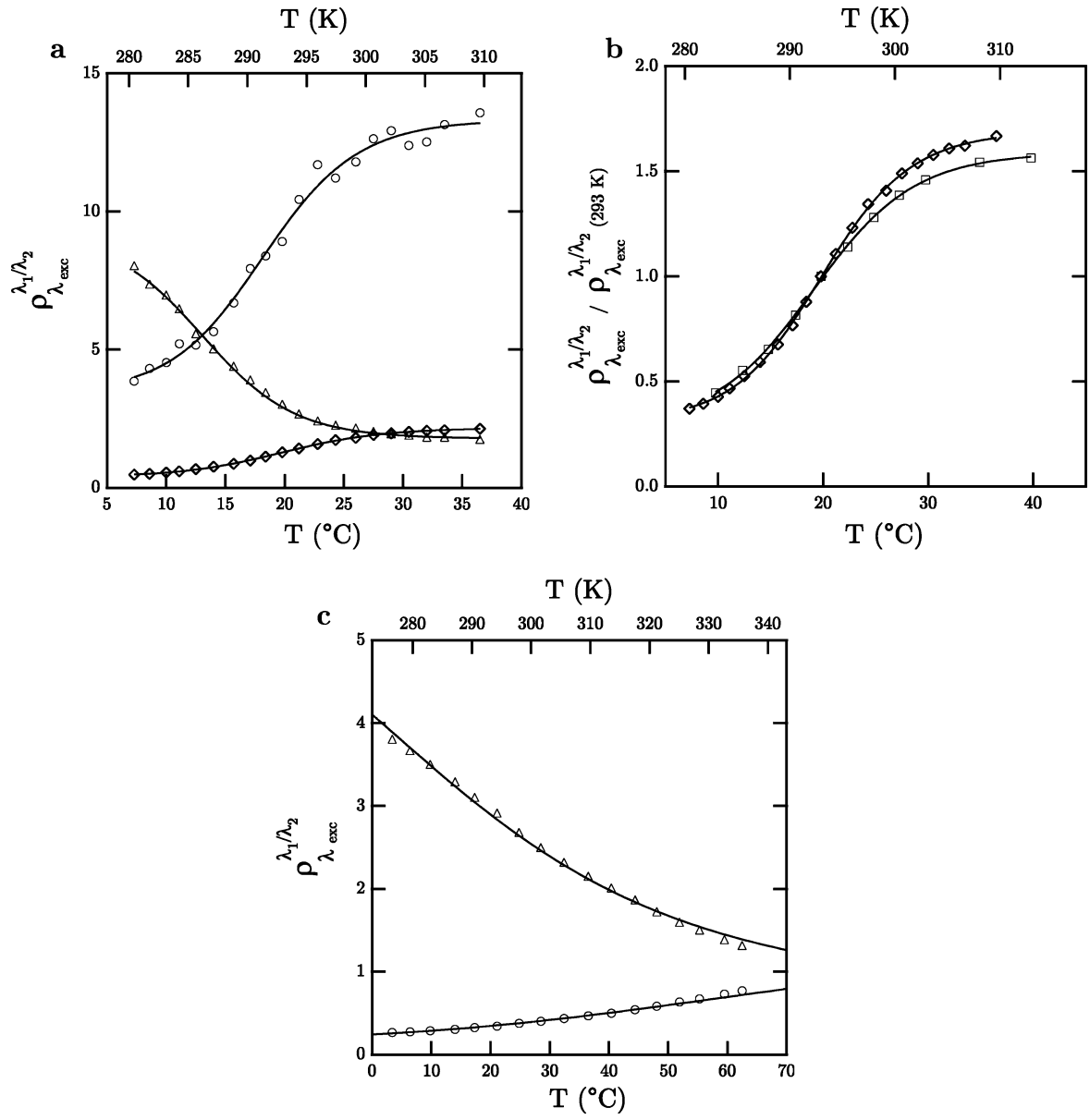

Figure 3. Temperature dependence of the $\rho^{\lambda_1/\lambda_2}_{\lambda_{exc}}$ ratio under various conditions of excitation and light collection. (a) Results for MB in 0.1 M NaCl 10 mM Hepes buffer, pH 7.5 at 20 °C, as measured using a spectrofluorimeter (○ corresponds to $\lambda_{exc} = 495$ nm, $\lambda_1 = 519$ nm, and $\lambda_2 = 700$ nm; Δ to $\lambda_{exc} = 495$ nm, $\lambda_1 = 611$ nm, and $\lambda_2 = 573$ nm; ◇ to $\lambda_{exc} = 495$ nm, $\lambda_1 = 518$ nm, and $\lambda_2 = 611$ nm). (b) Normalized ratio $\rho^{\lambda_1/\lambda_2}_{\lambda_{exc}}/\rho^{\lambda_1/\lambda_2}_{\lambda_{exc}}$(293 K) for MB in 0.1 M NaCl 10 mM Hepes buffer, pH 7.5 at 20 °C, as measured using a spectrofluorimeter (◇ to $\lambda_{exc} = 495$ nm, $\lambda_1 = 518$ nm, and $\lambda_2 = 611$ nm) or the dual-view microscope (□; band-pass filters such as $\lambda_{exc} = 480 \pm 20$ nm, $\lambda_1 = 535 \pm 25$ nm, and $\lambda_2 = 620 \pm 20$ nm). In the latter case the buffer was supplemented with 0.1% PDMA. (c) Results for PH in 5 mM monophthalate/diphthalate aqueous buffer, pH 5.2 at 20 °C, as measured using a spectrofluorimeter (○ corresponds to $\lambda_{exc} = 335$ nm, $\lambda_1 = 462$ nm, and $\lambda_2 = 530$ nm; Δ to $\lambda_{exc} = 335$ nm, $\lambda_1 = 530$ nm, and $\lambda_2 = 462$ nm). Markers correspond to experimental points. Solid lines correspond to fits to eqs 3 and 4 for MB ($\Delta_r H$, $T_{1/2}$, $Q^{\lambda_{exc},\lambda_{em}}_{A_1}$, and $Q^{\lambda_{exc},\lambda_{em}}_{A_2}$ being left as floating parameters) whereas for PH they correspond to calculations using the same equations (the temperature dependence of the thermometer brightnesses being from Figure S-5 in the Supporting Information and the thermodynamic parameters from the main text).

intensities of fluorescence emission. Because the latter measurement could be hampered by low signal-to-noise ratio, we have consequently been interested in investigating the dependence of $\rho^{\lambda_1/\lambda_2}_{\lambda_{exc}}$ with λ_1 and λ_2 associated with the maxima of emission of Fluorescein and Texas-Red, respectively. Thus, Figure 3a also displays $\rho^{518/611}_{495}(T)$. The 6.0×10^{-2} K^{-1} relative sensitivity we observed is only slightly smaller than the values obtained under the preceding optimized conditions; however, the signal-to-noise ratio is much improved as evidenced by less scattered experimental points.

In view of the application in thermal imaging by two-color epifluorescence microscopy, we eventually recorded the dependence of $\rho^{\lambda_1/\lambda_2}_{\lambda_{exc}}$ normalized to its value at 293 K, $\rho^{\lambda_1/\lambda_2}_{\lambda_{exc}}/\rho^{\lambda_1/\lambda_2}_{\lambda_{exc}}$(293 K), with the dual-view setup equipped with band-pass filters which mostly excite Fluorescein and essentially collect the emission from Fluorescein and Texas-Red, respectively ($\lambda_{exc} = 480 \pm 20$ nm, $\lambda_1 = 535 \pm 25$ nm, and $\lambda_2 = 620 \pm 20$ nm). As shown in Figure 3b, the correspond ing temperature dependence satisfactorily compares to the $\rho^{518/611}_{495}/\rho^{518/611}_{495}$(293 K) one recorded with the spectrofluo-

rimeter. The curve fits with eqs 3 and 4 provided $\Delta_r H = 166 \pm 5$ kJ mol^{-1} and $T_{1/2} = 288.1 \pm 0.1$ K (15.0 ± 0.1 °C) for the microscope data and $\Delta_r H = 169 \pm 4$ kJ mol^{-1} and $T_{1/2} = 288.4 \pm 0.1$ K (15.3 ± 0.1 °C) for the spectrofluorimeter ones. In particular, the fair agreement between the values of the thermodynamic parameters extracted with the two different setups underlines that, in the investigated temperature range, our microscope does not exhibit any significant dependence of its optical features on temperature.

Temperature Dependence of the PH Fluorescence Emission. Figure 2c displays the PH absorption spectrum at various temperatures in 5 mM sodium monophthalate/sodium diphthalate buffer, pH 5.2 at 20 °C. In contrast to MB, the dependence on T is well marked. The absorption band observed in the 300−400 nm range shifts toward shorter wavelengths upon heating. This behavior is in line with a progressive increase of the relative amount of the PYMPON basic state ($\lambda_{abs}^{max}A_2 = 326$ nm) over the PYMPON acidic state ($\lambda_{abs}^{max}A_1 = 355$ nm). This interpretation was confirmed by observing the corresponding evolution of the PH steady-state emission spectrum (Figure 2d). When the temperature increases, the emission in the wavelength range associated with the PYMPON acidic state ($\lambda_{em}^{max}A_1 = 530$ nm) drops whereas the one in the wavelength range associated with the PYMPON basic state ($\lambda_{em}^{max}A_2 = 462$ nm) rises. This behavior underlines the relevance of this pH probe to engineer an optical thermometer probe relying on a ratiometric analysis of the fluorescent emission.

Contrary to the situation encountered with the fluorophores born by MB, it is not possible to fit the data displayed in Figure 2d with eqs 2 and 3 in order to get the thermodynamic and photophysical features of PH. Indeed, $\rho_{\lambda_{exc}}^{\lambda_1/\lambda_2}$ is essentially linear on the temperature in the investigated range (see Figure 3c); and therefore, it does not exhibit enough sigmoidal shape to allow a reliable extraction of $\Delta_r H$ and $T_{1/2}$. In addition, the quantum yields of fluorescence of both PYMPON acidic and basic states significantly depend on temperature (Figure S-5a,b in the Supporting Information). Thus, we had to proceed differently to determine the thermodynamic and photophysical parameters characterizing the present thermometer. First, we extracted $\Delta_r H$ from the absorption data displayed in Figure 2c. More precisely, with the reference absorption spectra of the PYMPON acidic and basic states as well as the protonation constants of A_1 and $\mathscr{B}_1$ at 298 K, we calculated the evolution of the absorption spectrum on temperature for several values of the enthalpy of the reaction in eq 1, and we retained the closest to the experimental behavior. We found $\Delta_r H = 44 \pm 4$ kJ mol^{-1}, which subsequently gave access to $T_{1/2} = 321 \pm 1$ K (48 ± 1 °C) (Figure S-6a in the Supporting Information). Taking into account that $\Delta_{\mathscr{B}_1} H = -2.2$ kJ mol^{-1},[75] we deduced $\Delta_{A_1} H = 42 \pm 4$ kJ mol^{-1}. One may notice that this value is significantly larger than the corresponding 18.2 kJ mol^{-1} value observed for the parent pyridinium headgroup.

Equipped with the preceding information and assuming that both PYMPON acidic and basic states do not see the shape of their emission spectrum varying with T (see Figure S-5a,b in the Supporting Information), we eventually relied on eq 2 to derive from Figure 2d the temperature dependence of both species quantum yields. More precisely, the evolution of the PH emission spectrum upon heating was calculated by adopting the empirical law[65] $\ln(1/\phi_{A_i} - 1) = \ln(\alpha_{A_i}) - \beta_{A_i}/T$ (see Figure S-6b in the Supporting Information) and subsequently compared to Figure 2d data. The best fit yielded $\alpha_{A_1} = 105 \pm 10$, $\beta_{A_1} = 1640 \pm 100$ K, $\alpha_{A_2} = 2140 \pm 100$, and $\beta_{A_2} = 2700 \pm 100$ K. Incidently, these latter values are in good agreement with independent measurements performed on either the A_1 or the A_2 state alone (Figure S-5c in the Supporting Information).

Because we could not reliably assume $|2RT_i/\Delta_r H| \ll 1$ for PH and because the PYMPON acidic and basic states present temperature dependent quantum yields, we could not follow the procedure used with MB to perform the excitation and emission wavelengths optimization necessary to achieve optimal sensitivity in temperature measurements. In particular, as $T_{1/2}$ was clearly exceeding room temperature, we did not attempt to perform the optimization at T_i. To benefit from a large signal-to-noise ratio, we first adopted $\lambda_{exc} = 335$ nm, which corresponds to the isosbestic point where both PYMPON acidic and basic states strongly absorb (Figure 2c). Then, using eq 2, we calculated the total fluorescence intensity at various emission wavelengths in the [400 nm, 600 nm] range and correspondingly obtained the variation of $\rho_{\lambda_{exc}}^{\lambda_1/\lambda_2}$ as a function of λ_1 and λ_2. This process was repeated at various temperatures; it therefore allowed us to compute, by numerical differentiation of $\rho_{\lambda_{exc}}^{\lambda_1/\lambda_2}$ with respect to T, the dependence of $(\rho_{\lambda_{exc}}^{\lambda_1/\lambda_2})'$ on λ_1 and λ_2. Figure S-7a,b in the Supporting Information displays the results obtained at 25 °C. They show that two $\{\lambda_1,\lambda_2\}$ pairs, {530 nm,400 nm} and {456 nm,600 nm}, provide the largest absolute values for $(\rho_{\lambda_{exc}}^{\lambda_1/\lambda_2})'$ (they, respectively, correspond to a minimum and maximum). A similar behavior was found at any temperature between 10 and 60 °C. Furthermore, in all the optimized $\{\lambda_1,\lambda_2\}$ couples, one wavelength was close to the maximum of emission of either the acidic or basic PYMPON state. In contrast, the other one was located at the border of the investigated wavelength range, where the difference of brightness between A_1 and A_2 is at the highest. However, as such situations could be associated with low intensities of fluorescence emission, resulting in a poor signal-to-noise ratio, we have eventually considered retaining the maxima of fluorescence emission for both PYMPON states to evaluate the efficiency of PH as a thermometer. Figure 3c, thus, displays the temperature dependence of $\rho_{335}^{462/530}$ and $\rho_{335}^{530/462}$. Both curves vary smoothly between 10 and 60 °C. In the corresponding temperature range, $(\rho_{335}^{462/530})'/\rho_{335}^{462/530}$ and $(\rho_{335}^{530/462})'/\rho_{335}^{530/462}$ are essentially constant and, respectively, equal to 1.8×10^{-2} and -1.7×10^{-2} K^{-1} at 298 K.[78]

Implication of the Thermometers Response Times for Dynamic Measurements. Beyond illustrating the strategy for temperature determination relying on a nonathermal reaction, the MB and PH systems were envisaged for facing various experimental situations. Whereas both optical thermometers could be equally used for steady-state measurements, they were anticipated to exhibit distinct dynamic behavior with respect to temperature changes. Indeed, the relaxation times associated with both conformational transition and proton exchange are significantly different.

On the basis of previously reported FCS investigations on similar oligonucleotides,[79] the characteristic time for beacon opening was expected to lie in the 0.1−1 ms range. In this study, we also retained FCS to measure the kinetics associated with MB conformational changes (see the Supporting Information).[79,80] With the use of a homemade setup,[81,82] the fluctuations of the Fluorescein emission at 296 K in 0.1 M NaCl 10 mM Hepes buffer pH 7.5 yielded 21 ± 4 μs for the relaxation time of the eq 1 reaction. Then relying on the K value derived from Figure 2b, we extracted $(3.8 \pm 0.8) \times 10^4$ s^{-1} and $(9 \pm 1) \times 10^3$ s^{-1} for the rate constants associated with the opening and closing steps, respectively. Noticeably, the latter result is in fair agreement with the literature ones.[79] In the present context, the measured relaxation time value shows that MB can reliably be used for thermometry around room temperature up to the kilohertz range. Incidentally, we also measured a $(7.2 \pm 0.7) \times 10^{-11}$ m^2 s^{-1} diffusion coefficient for MB, which compares well with the $(6.8 \pm 0.3) \times 10^{-11}$ m^2 s^{-1} value obtained by on-chip concentration profile analysis (see the Supporting Information).[83]

We had previously measured by FCS the rate constants for some proton exchanges involving PYMPON.[82] In particular, we found $(1.5 \pm 0.2) \times 10^{10}$ M^{-1} s^{-1} for the protonation rate of the PYMPON basic state by free protons. Adopting the latter value for the protonation by the acidic state of the monophthalate buffer B_1,[84] we could derive an order of magnitude for the relaxation time associated with PYMPON protonation: it should be in the 2 μs range in the presence of about 5 mM monophtalate buffer at pH = p$K_a(B_1)$. Thus, the PH system is expected to allow for reliable thermometry up to 1 MHz, a much higher frequency range than the one that can be reached by MB. Hence, although exhibiting less favorable thermodynamic and photophysical features, PH should prove better than MB to analyze very fast temperature changes.

Two-Color Thermal Imaging of a Solution Heated by a Resistive Strip. After having thoroughly characterized the behavior of MB and PH in relation to thermometric applications, we have been interested to use them for thermal imaging in a microsystem filled with aqueous solutions. In this report, we focus on steady-state temperature profiles and therefore we could adopt MB, which exhibits the highest sensitivity (vide supra). The analysis of temporally varying thermal maps has been left for a future publication.

More specifically, we selected a simple 130 μm thick microfluidic chamber locally heated by a thin film resistor to illustrate temperature measurements by ratiometric imaging of the fluorescence emission at two different wavelengths. The device was made of a glass slide on which a 800 μm long and 20 μm large ITO heater had previously been fabricated. Parafilm strips were used as spacers and a glass coverslip as a lid. We limited current injection in order to increase the semiconductor temperature by only a few degrees. Considering the small temperature coefficient of this material ($\sim 7 \times 10^{-4}$ K^{-1}), we could assume its resistivity to remain constant upon heating and thus the Joule effect to be homogeneous. Moreover, taking into account the small thickness of the film, we finally modeled the resistive strip as an infinitely thin boundary on which a uniform heat flux was generated. Both analytical and FEM computations were accordingly simplified (see the Supporting Information). For instance, we could show that the temperature relaxation around the ITO strip axis is roughly logarithmic, as one would expect for radial heat transfer in a hollow cylinder.[85]

In the preceding considerations on heat exchange in the microsystem, water has been considered as a solid although horizontal temperature gradients necessarily generate natural convection. However, for an ITO strip heated by less than 5 °C above the microscope stage setting, the flow velocity is less than 1.7 μm s^{-1}, consequently yielding a thermal Peclet number smaller than 1 (1.5×10^{-3} here); fluid particles are thermostatted during their motion and indeed one does not need to consider water recirculations when computing the temperature field in the observation cell (see the Supporting Information).

Figure 4 displays the successive steps leading to the thermal map. With the present microscope, this measurement is representative of the probe response averaged along the optical axis, i.e., along z. More precisely, Figure 4a shows the source image originating from a device filled with a 2 μM MB solution in 0.1 M NaCl 10 mM Hepes buffer, pH 7.5 at 20 °C, supplemented with 0.1% PDMA. With the use of a dual-view setup, it is possible to record both green and red channels with a single CCD camera (see Experimental Section and Scheme S-2 in the Supporting Information). Subtraction of the background noise is then performed before dividing the green image by the red one. By taking the ratio of the fluorescence emission at two wavelengths, we can obtain a measurement independent from inhomogeneities in probe concentration and excitation power. However, the result still depends on spatial variations in photon collection efficiency (see eq 24 in the Supporting Information). Consequently, an additional normalization step has to be performed: the latter ratiometric thermal image is divided by a second one that has been acquired in conditions where the whole device is at the same temperature. In the present experiment we just had to stop injecting current in the resistor to obtain the microsystem thermostatation at 293 K. Finally, it gives Figure 4b data which corresponds to the $\rho^{\lambda_1/\lambda_2}_{\lambda_{exc}}(x,y) / \rho^{\lambda_1/\lambda_2}_{\lambda_{exc}}(293\ \mathrm{K})$ map. As for the considered molecular thermometer and the considered optical setup, the $\rho^{\lambda_1/\lambda_2}_{\lambda_{exc}}(T)$ calibration curve has already been measured (see Figure 3b), it now becomes straightforward to extract temperature profiles from the normalized ratiometric image. Thanks to the narrow working range, we could here assume a MB response linearly depending on T, associated with a 6.0×10^{-2} K^{-1} relative sensitivity at 293 K.

To validate our method, we compared the experimental z-averaged temperature field measured by two-color fluorescence microscopy with predictions provided by FEM simulations (Figure S-8b in the Supporting Information). The latter computations were performed in 2D, only considering the cross-sectional (y,z)-plane,

(79) Bonnet, G.; Krichevsky, O.; Libchaber, A. *Proc. Natl. Acad. Sci. U.S.A.* **1998**, *95*, 8602–8606.
(80) Jung, J.; Van Orden, A. *J. Am. Chem. Soc.* **2006**, *128*, 1240–1249.
(81) Gosse, C.; Boutorine, A.; Aujard, I.; Chami, M.; Kononov, A.; Cogné-Laage, E.; Allemand, J.-F.; Li, J.; Jullien, L. *J. Phys. Chem. B* **2004**, *108*, 6485–6497.
(82) Charier, S.; Meglio, A.; Alcor, D.; Cogné-Laage, E.; Allemand, J.-F.; Jullien, L.; Lemarchand, A. *J. Am. Chem. Soc.* **2005**, *127*, 15491–15505.
(83) Estévez-Torres, A.; Gosse, C.; Le Saux, T.; Allemand, J.-F.; Croquette, V.; Berthoumieux, H.; Lemarchand, A.; Jullien, L. *Anal. Chem.* **2007**, *79*, 8222–8231.
(84) Eigen, M. *Angew. Chem.* **1963**, *75*, 489–508.
(85) Van Keuren, E.; Littlejohn, D.; Schrof, W. *J. Phys. D: Appl. Phys.* **2004**, *37*, 2938–2943.

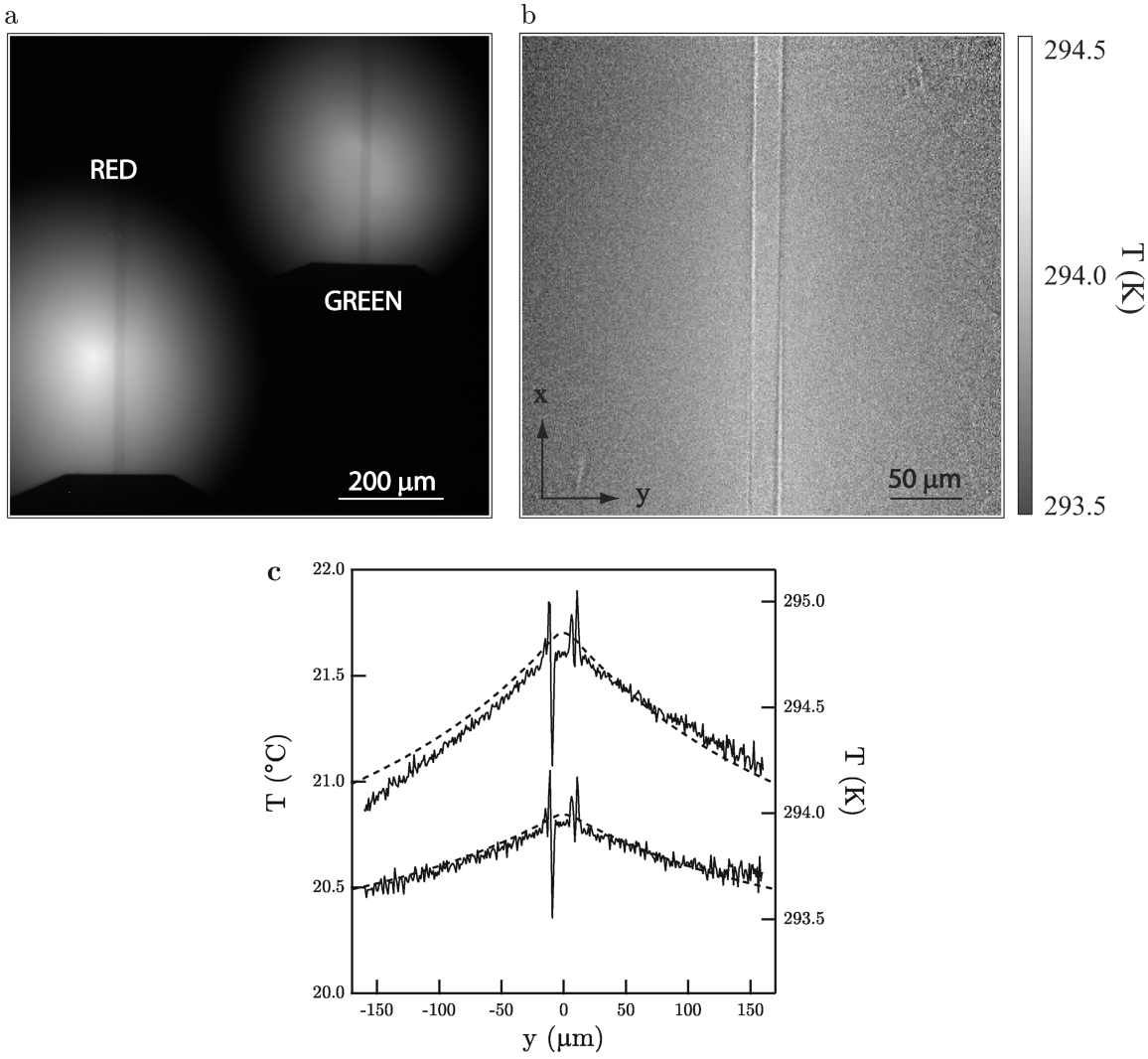

Figure 4. Two-color temperature mapping of a microfluidic chamber heated by Joule effect, a constant current *i* flowing into a 20 μm large ITO strip that has been fabricated onto the lower substrate of the device. Measurements were performed using MB at 2 μM in 0.1 M NaCl 10 mM Hepes buffer, pH 7.5 at 20 °C, supplemented with 0.1% PDMA. The device holder was thermostatted at 293 ± 0.2 K. (a) Thermal image $\mathcal{T}^{\lambda_1,\lambda_2}_{\lambda_{exc}}(x,y)$ as acquired with the camera, upon injecting $i = 2.00$ mA. The fluorescence emission intensity profiles corresponding to both green and red channels are recorded simultaneously on the same CCD chip. (b) Corresponding normalized ratiometric image $\mathcal{R}^{\lambda_1/\lambda_2}_{\lambda_{exc}}(x,y)/\mathcal{R}^{\lambda_1/\lambda_2}_{\lambda_{exc},293K}(x,y)$ from which the temperature field can be retrieved using the $\rho^{\lambda_1/\lambda_2}_{\lambda_{exc}}(T)$ calibration curve displayed with squares in Figure 3b (conversion of gray levels into degrees Celsius is linear in the operating range). After subtraction of the background noise, the green and red channels have been divided by each other to yield a ratiometric image that was subsequently normalized by the one obtained at zero current (see Supporting Information). (c) Temperature profiles along the *y*-axis for two different values for the current *i*, 2.83 (top) and 2.00 mA (bottom). Solid lines account for measurements and dashed lines for the corresponding FEM simulations (in both cases the temperature was averaged over the whole water layer thickness). To increase the signal-to-noise ratio, the experimental data were *x* -averaged over 300 μm around the heater center. Additionally, the simulated data were shifted 0.15 K upward to better match measurements (see main text).

i.e., the one normal to the strip main axis. Indeed, we assumed the ITO heater to be infinitely long, a reasonable approximation in relation to the present geometry.[86] Correspondingly, the measured thermal map was averaged over 300 μm along the *x*-axis in order to increase the signal-to-noise ratio. Figure 4c displays, for two different current intensities ($i = 2.00$ and 2.83 mA), the experimental and the calculated (x,z)-averaged temperature profiles in the microchamber.[87] Both results are in good agreement provided 0.15 K were added to the simulated data, a small discrepancy that the limited accuracy of the thermocouple can easily account for. Hence, these data strongly support MB as a reliable fluorescent temperature probe for ratiometric dual-emission-wavelength imaging in aqueous solutions.

CONCLUDING REMARKS

In this article, we systematized the design of unimolecular fluorescent thermometers for ratiometric dual-emission-wave-

(86) The length of the ITO strip is $\ell = 800$ μm whereas, according to theoretical and FEM estimates, the thermal relaxation in the (x, z)-plane is altered by the edges presence only over $\ell_{long} \sim 5-250$ μm (see Supporting Information). Additionally, temperature variations observed by two-color thermometry span over less than ~100 μm from the gold contacts. Thus, the finite nature of the heater will not be seen if thermal imaging is performed around the strip center.

(87) The spikes and dips observed on the measured temperature profile originate from the manual procedure used for video data treatment. Indeed, to obtain the ratiometric image, one has to divide the green and red channel views by each other and sharp signal variations are observed if the alignment of the heater edges is not perfectly achieved.

length measurements in aqueous solutions. As an application, we imaged temperature profiles in a microfluidic device without any a priori knowledge of the probe concentration and using only widely available chemicals and optical setup.

Our strategy relies on molecules involved in a nonathermal reaction and which exchanging states display different emission characteristics. Generic engineering rules were derived to optimize the probe thermodynamics features and the observation settings with respect to a desired operating temperature range and a maximum sensitivity. In particular, molecular beacon-based fluorescent thermometers can reliably be designed to work at various temperatures: one just needs to select the appropriate sequence length and composition.[11,55,88] Likewise, the wavelengths used for measurements can be tuned by choosing the suitable fluorophores. Interestingly the elaboration of such probes is today facilitated by the existence of numerous predictive tools[73] and commercial sources. On the other hand, for extremely fast two-color temperature measurements, a second chemical platform was proposed, which associates a ratiometric fluorescent pH probe and a buffer.

The present series of molecules can be applied to microsystem thermal imaging without any demanding equipment. For instance, we demonstrated that using a simple epifluorescence microscope equipped with a single CCD camera, the molecular beacon-based probe could provide the whole temperature field in a microfluidic cell heated by a resistive strip. Although measurements were here averaged along the optical axis, it would be easy to implement our method in the third dimension by working on a confocal or a two-photon microscope. Like in fluorescence lifetime imaging, one would thus obtain 3D temperature profiles independent of experimental parameters such as dye concentration or excitation/detection efficiency.[89]

Finally, despite this work only reports on steady-state temperature mapping, our results suggest that the present strategy is fully compatible with dynamic temperature imaging. Care should just be taken when selecting a thermometer: molecular beacons have response times around the millisecond range, whereas pH probes can reach the microsecond range.

ACKNOWLEDGMENT

We thank S. Charier and B. Goetz (ENS, Paris) for the PYMPON synthesis and O. Jouannot, D. Pujade, G. Philippe, and J.-Y. Faou for punctual help in experiments. C. Bergaud (LAAS, Toulouse), J.-F. Allemand and V. Croquette (ENS, Paris), A. Lemarchand (UPMC, Paris), S. Volz (ECP, Châtenay-Malabry), J.-L. Mergny, and L. Lacroix (MNHN, Paris) are acknowledged for insightful discussions. We are also indebted to the following people for their technical assistance: J. Quintas da Silva (ENS), N. Allemandou, G. Chanconie, and L. Merzeau (LPN) for mechanics; and L. Leroy, L. Couraud, D. Chouteau, X. Lafosse, J.-C. Esnault, C. Ulysse, and S. Guilet (LPN) for microfabrication. This work was supported by the "T-Wave" grant from the 2006 "ANR Blanche" program.

SUPPORTING INFORMATION AVAILABLE

Derivation of the inflection and of the maximum sensitivity value for both one-color and two-color thermometers, the procedure used for data treatment in ratiometric thermal mapping, the derivation of the quantum yields of energy transfer in MB, the description and the analysis of the FCS experiments on MB including the MB diffusion coefficient measurement in a microsystem, a detailed analysis of heat transfer in the microdevice, the description of the FEM simulations, three complementary schemes, and nine complementary figures; the schemes display the structure of the labeling terminal fluorophores borne at the ends of the molecular beacon MB, the overall structure of the microdevice, the optical setup for two-color epifluorescence imaging, and the device employed to validate the use for thermal mapping of the MB ratiometric temperature probe; the figures display the dependence of the steady-state normalized fluorescence emission of MB models on temperature, the theoretical evaluation for MB of T_i and $(\rho_{\lambda_{exc}}^{\lambda_1/\lambda_2})'(T_i)$ as functions of the wavelengths of fluorescence emission λ_1 and λ_2, FCS autocorrelation curves recorded on MB solutions, the dependence on temperature of the emission spectra of both PH acidic and basic states, the calculation of the PH absorption and emission spectra at various temperatures (in order to determine the thermometer thermodynamic and photophysical parameters), the theoretical evaluation for PH of $(\rho_{\lambda_{exc}}^{\lambda_1/\lambda_2})'$ as a function of λ_1 and λ_2, the FEM simulations of the temperature field in the microchamber incorporating on its bottom an ITO wire heated at constant current i, and the dependence of the ratiometric behavior of both MB and PH during a whole cooling−heating sequence (in order to evidence the reversibility of their response to temperature changes). This material is available free of charge via the Internet at http://pubs.acs.org.

Received for review May 12, 2009. Accepted July 17, 2009.

AC901027F

(88) Bourdoncle, A.; Estèvez-Torres, A.; Gosse, C.; Lacroix, L.; Vekhoff, P.; Le Saux, T.; Jullien, L.; Mergny, J.-L. *J. Am. Chem. Soc.* **2006**, *128*, 11094–11105. As demonstrated in this reference, it is also possible to devise oligonucleotide probes which operating temperature range can be adjusted by simply varying the buffer composition.

(89) Two-color mapping has the advantage of setup simplicity whereas FLIM-based techniques rely on more straightforward measurement procedures. For instance, no background image acquisition is necessary with the latter technique.